





Cite this: DOI: 10.1039/d5an00647c

A dual-ion-selective electrode system for real-time monitoring of dissolved ammonia

Ayman H. Kamel  ^{a,b} and Hisham S. M. Abd-Rabboh  ^c

A robust, all-solid-state potentiometric sensor was developed for the selective detection of dissolved ammonia (NH₃) in aqueous and gas-equilibrated environments. The sensor design is based on a coupled configuration of a nonactin-based ammonium-selective electrode (NH₄⁺-ISE) and a hydrogen ion-selective electrode (H⁺-ISE), enabling direct measurement of NH₃ activity through the equilibrium: NH₄⁺ ⇌ NH₃ + H⁺. The resulting electrochemical cell exhibited a near-Nernstian response over a wide dynamic range, with a detection limit below 10 ppm and a response time under 6 seconds. In contrast to conventional membrane-based gas sensors, the dual-electrode system showed minimal signal drift and eliminated the need for gas-permeable membranes or internal filling solutions. Sensor performance was evaluated under various pH and ionic strength conditions, confirming matrix-independent behavior and suitability for direct application in complex environmental samples such as seawater and wastewater. The sensor also demonstrated excellent reversibility and real-time monitoring capability during dynamic NH₃ fluctuation experiments in a freshwater aquaculture system, successfully tracking diurnal changes linked to photosynthetic and respiratory activity. A comparison with a commercial Severinghaus-type ammonia gas probe revealed significantly enhanced stability, faster response, and improved reproducibility for the proposed device. This dual-ion-selective electrode system offers a practical and high-performance platform for on-site NH₃ detection in environmental, aquacultural, and biological monitoring applications.

Received 14th June 2025,
Accepted 6th August 2025

DOI: 10.1039/d5an00647c

rsc.li/analyst

Introduction

Ammonia (NH₃) is a key component in the biogeochemical nitrogen cycle and a critical indicator of water quality in aquatic environments. In its un-ionized form, ammonia is toxic to aquatic life, impairing respiration and disrupting enzymatic processes at concentrations as low as 0.02–0.05 mg L^{−1}.¹ In natural and engineered systems, ammonia exists in equilibrium with its conjugate acid, the ammonium ion (NH₄⁺), and the NH₃/NH₄⁺ ratio is highly dependent on pH and temperature.² Accurate measurement of dissolved NH₃, rather than just total ammoniacal nitrogen (TAN), is essential for effective environmental monitoring, regulatory compliance, and toxicity assessment.³

Monitoring ammonia in aqueous media presents substantial analytical challenges. Conventional methods such as the indophenol blue colorimetric method, flow injection analysis, or fluorimetric techniques are often time-consuming, require

hazardous reagents, and are poorly suited for *in situ* deployment.^{4–7} Ammonia gas-sensing electrodes—typically based on Severinghaus-type configurations—incorporate gas-permeable membranes and alkaline internal solutions to measure NH₃ indirectly *via* pH changes. While effective under controlled conditions, these sensors are susceptible to membrane fouling, long equilibration times, evaporation of internal solutions, and cross-sensitivity to volatile acids such as CO₂.^{8–10}

Electrochemical sensors, particularly ion-selective electrodes (ISEs), offer an attractive alternative for the detection of ionic species in environmental samples due to their low cost, operational simplicity, and compatibility with real-time and field measurements.^{11–13} Unlike spectrophotometric methods, ISEs convert ion activity directly into an electrical potential, enabling fast and reagent-free detection. Ammonium-selective electrodes using nonactin as the ionophore have been widely developed for this purpose; however, their selectivity is often compromised by the presence of interfering alkali cations such as Na⁺ and K⁺, especially in high-ionic-strength matrices such as seawater or wastewater.^{14–16}

Traditional liquid-contact ISEs suffer from limitations related to mechanical fragility, internal solution evaporation, and long-term instability.^{17–20} These limitations have largely been overcome by the development of solid-contact ion-selective

^aDepartment, College of Science, University of Bahrain, Sakhir 32038, Kingdom of Bahrain. E-mail: ahkamel76@sci.asu.edu.eg^bChemistry Department, College of Science, King Khalid University, PO Box 9004, Abha, 62223, Saudi Arabia^cDepartment of Chemistry, Faculty of Science, Ain Shams University, Cairo 11566, Egypt

electrodes (SC-ISEs), which replace the internal liquid junction with an ion-to-electron transduction layer—often composed of hydrophobic polymers, carbon nanomaterials, or conducting polymers such as PEDOT:PSS—thereby improving signal stability, miniaturization, and operational durability.^{21–26} The improved analytical performance and fabrication simplicity of SC-ISEs make them highly suitable for continuous monitoring in complex environmental matrices.^{12,26,27}

Nevertheless, a single ammonium-selective electrode cannot directly report the concentration of un-ionized NH_3 , as the equilibrium between NH_4^+ and NH_3 is governed by the solution's proton activity. Consequently, changes in pH can shift the speciation dramatically without altering the total ammonia content. Without real-time pH compensation, these shifts can lead to significant misinterpretation of NH_3 levels.^{28,29} While some systems attempt to integrate separate pH measurements, they often rely on bulky or fragile glass electrodes, which are not well suited for compact or integrated sensor platforms.³⁰ Recent strategies have employed dual-electrode potentiometric systems to overcome this problem. By coupling two SC-ISEs—one selective for NH_4^+ and the other for H^+ —the system can exploit the chemical equilibrium:



to calculate dissolved NH_3 activity from the potential difference between the two electrodes. This configuration offers real-time, matrix-independent, and reversible sensing of ammonia without the need for gas diffusion membranes or internal filling solutions.^{31,32} Such dual-sensor designs have previously shown success in CO_2 sensing by pairing carbonate- and pH-selective electrodes to extract CO_2 activity from the equilibrium relationships among dissolved inorganic carbon species.³³

Moreover, the integration of these electrodes into screen-printed platforms offers additional advantages. Screen-printed solid-contact electrodes (SP-SC-ISEs) enable cost-effective mass production, miniaturization, and deployment in remote or portable monitoring systems.^{34–36} Modified transducer layers, including reduced graphene oxide (rGO), carbon nanotubes (CNTs), and hydrophobic polymer composites, have shown notable improvements in detection limits, stability, and resistance to interfacial water layer formation—major sources of potential drift in conventional SC-ISEs.^{26,27,37}

In this study, a dual solid-contact ion-selective electrode (DISE) system is proposed for the real-time monitoring of dissolved ammonia. The system consists of screen-printed NH_4^+ - and H^+ -selective electrodes fabricated using nonactin and tri-dodecylamine as respective ionophores. The electrode potentials are used to extract NH_3 activity directly from the $\text{NH}_4^+/\text{NH}_3/\text{H}^+$ equilibrium without requiring any chemical conversion, gas separation, or membrane conditioning. The performance of the system is evaluated in terms of Nernstian response, selectivity, potential drift, and detection limit, and benchmarked against a commercial Severinghaus-type ammonia sensor to demonstrate its operational advantages in terms of

response time, stability, and compatibility with high-ionic-strength matrices. In the absence of a classical reference electrode, the H^+ -ISE acts as a functional pseudo-reference in the dual-ISE system, enabling differential measurement of NH_3 activity through its equilibrium with NH_4^+ and H^+ .

While prior dual-ISE systems have been used for gas-phase analytes like CO_2 ,^{31–33} they often rely on non-integrated or fragile platforms. This study presents the first robust, screen-printed, miniaturized platform using all-solid-state electrodes for direct potentiometric measurement of NH_3 . The elimination of internal buffers or membranes makes the system more suitable for environmental deployment.

Experimental section

Apparatus

A commercial Ag/AgCl reference electrode was used only in the standalone NH_4^+ -ISE calibration experiments for comparison purposes. In the dual-electrode ammonia sensing configuration, no external reference was used. For comparison, potentiometric measurements were also conducted using a commercial ammonia gas sensor (Orion, Thermo Fisher Scientific). All potential measurements were performed at room temperature (22 ± 1 °C) using a portable potentiometric analyzer (PalmSens 4, PalmSens BV, The Netherlands) with high-impedance input and customized LabVIEW-based data acquisition software.

Chemicals and reagents

All reagents were of analytical grade and used as received without further purification. Poly(vinyl chloride) (PVC, high molecular weight), *o*-nitrophenyl octyl ether (*o*-NPOE), tetrahydrofuran (THF), and the ionophore nonactin were purchased from Sigma-Aldrich (St Louis, MO, USA). The hydrogen ion-selective ionophore (ETH 2412) was obtained from Fluka (Buchs, Switzerland). Potassium tetrakis(4-chlorophenyl) borate (KTpClPB) was used as a lipophilic additive in selected membrane formulations to improve charge transfer properties. To fabricate the ion-to-electron transducing layer, two different materials were investigated: poly(3,4-ethylenedioxythiophene) polystyrenesulfonate (PEDOT:PSS), and multi-walled carbon nanotubes (MWCNTs). All carbon nanomaterials were procured from Sigma-Aldrich and were used to modify glassy carbon electrode surfaces prior to membrane casting. Tris buffer (50 mM, pH 7.2) was used in all experiments due to its buffering capacity near neutral pH. Control measurements in Tris buffer alone confirmed no significant interaction between Tris and either ion-selective membrane. This buffer system ensured consistent pH conditions suitable for comparative studies between all-solid-state ion-selective electrodes (ISEs) and a traditional gas-sensing setup using Ag/AgCl reference electrodes. A 0.1 M ammonium chloride (NH_4Cl) stock solution was prepared in deionized water (18.2 MΩ cm, Milli-Q system, Millipore, Bedford, MA, USA), and diluted with Tris- H_2SO_4 buffer to prepare calibration standards in the desired concentration range.

Electrode fabrication

Screen-printed electrodes (SPEs) were fabricated in-house on flexible polyethylene terephthalate (PET) substrates. A copper-based conductive ink (Sigma-Aldrich, product #773705) was screen-printed to define the working electrode tracks and contact pads. The printed substrates were then thermally cured at 120 °C for 30 min under a nitrogen atmosphere to ensure conductivity and minimize oxidation. Each copper electrode surface was modified with a specific ion-to-electron transducing material to evaluate its impact on sensor performance. PEDOT:PSS (1.3 wt% aqueous dispersion), and MWCNTs (0.5 mg mL⁻¹) in DMF were individually drop-cast (5 µL) onto the copper disk and left to dry under ambient conditions. PEDOT:PSS was selected for its low impedance and electrochemical stability, while MWCNTs were chosen for their hydrophobicity and high double-layer capacitance. These characteristics help suppress potential drift and water layer interference. The ion-selective membrane cocktail was composed of 33 wt% PVC, 66 wt% *o*-NPOE, 1.5 wt% ionophore (nonactin for NH₄⁺ or ETH 2412 for H⁺), and 0.5 wt% KTpClPB, dissolved in THF. A 10 µL aliquot of this membrane solution was carefully drop-cast onto the dried transducer layer and allowed to evaporate overnight in a clean environment.

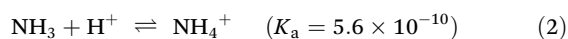
The electrodes were conditioned in 1.0 mM NH₄Cl or 1.0 mM HCl (depending on the ion-selective membrane) for 24 h prior to use to stabilize their electrochemical response. Sensors were calibrated in NH₄Cl solutions (10⁻⁷–10⁻³ M) buffered to pH ~7.2 using NH₃/NH₄⁺ buffer to promote equilibrium. Response time was assessed by rapid concentration jumps. Interference studies were carried out using equimolar solutions of K⁺, Na⁺, and Ca²⁺. For environmental relevance, aquarium water was used for real-time NH₃ monitoring under light/dark cycles.

Results and discussion

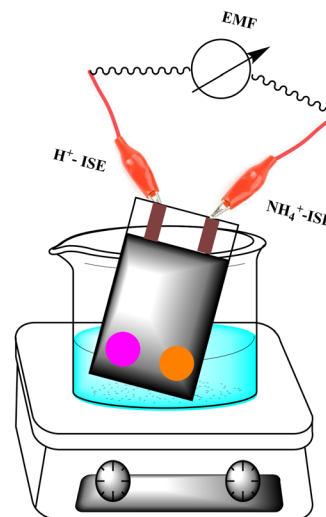
Sensor working principle

The solid-state ammonia sensor consists of an all-solid-state H⁺-selective electrode (H⁺-ISE) and a solid-state NH₄⁺-selective electrode (NH₄⁺-ISE) arranged in a closed electrochemical cell configuration (Scheme 1). This setup eliminates the need for a traditional liquid-junction reference electrode. The potential difference (EMF) generated between the H⁺-ISE and the NH₄⁺-ISE reflects the partial pressure of dissolved ammonia (NH₃) in the sample solution at equilibrium.

Ammonia dissolved in aqueous solution is governed by the acid–base equilibrium:



At equilibrium, the activities of NH₃, NH₄⁺, and H⁺ are related through the known dissociation constant K_a . Because the electrodes are selective for NH₄⁺ and H⁺ ions respectively, the EMF of the electrochemical cell is thermodynamically linked to the activity of dissolved NH₃ as:



Scheme 1 Schematic illustration of the dual-ion-selective electrode (DISE) configuration using an NH₄⁺-selective electrode (NH₄⁺-ISE) and a hydrogen ion-selective electrode (H⁺-ISE) acting as a pseudo-reference.

$$\text{EMF} = E_{\text{NH}_4^+} - E_{\text{H}^+} = K' + \log(a_{\text{NH}_4^+}/a_{\text{H}^+}) \quad (3)$$

Using the equilibrium relation:

$$K_a = a_{\text{NH}_4^+}/a_{\text{NH}_3} \cdot a_{\text{H}^+} \quad (4)$$

Substituting into the Nernst equation gives:

$$\text{EMF} = K'' + \log[a_{\text{NH}_3}] \quad (5)$$

where K'' [$K'' = E_{\text{NH}_4^+}^0 - E_{\text{H}^+}^0 + 0.059 \log K_a$] is a combined constant that includes electrode-specific potential and equilibrium constant.

It should be noted that in this dual-electrode configuration, the H⁺-ISE acts as a functional pseudo-reference electrode, and the measured EMF reflects the potential difference governed by the NH₄⁺/NH₃/H⁺ equilibrium. Despite potential selectivity concerns, ETH 2412 exhibits minimal cross-sensitivity under buffered environmental conditions. This configuration, while reference-free, remains thermodynamically valid and provides stable ammonia readout in most real-world matrices. Thus, the sensor response is directly proportional to the logarithm of the dissolved ammonia activity without the need for extra thermodynamic assumptions or an external reference electrode. This configuration is particularly suitable for real-time environmental monitoring of dissolved NH₃ in seawater and other alkaline samples, where the NH₄⁺/NH₃ equilibrium shifts toward volatile ammonia.

Potential response characteristics

The calibration behavior of the developed potentiometric NH₃ sensor is summarized in Fig. 1. The slope values were found to be 59.2 mV per decade and 54.3 mV per decade for the NH₄⁺-ISE and H⁺-ISE, respectively. The sensor employs a nonactin-based ammonium-selective membrane electrode (NH₄⁺-ISE) coupled with a solid-state H⁺-ISE to construct an all-solid-state

electrochemical NH_3 sensor. This dual-electrode configuration enables direct potentiometric measurement of ammonia activity *via* the equilibrium shown in eqn (1). Three independent calibration strategies were employed to evaluate sensor performance across liquid, gas-equilibrated, and dry gas conditions, simulating different environmental and industrial scenarios.

Aqueous NH_4Cl solution calibration (liquid phase). In this setup, the sensor was immersed directly into buffered NH_4Cl solutions of known concentrations (10^{-3} , 10^{-4} , 10^{-5} , and 10^{-6} M) at pH 7.2. At this pH, the equilibrium favors NH_4^+ , and only a small fraction exists as free NH_3 . Thus, the EMF response is indirectly governed by the dissociation equilibrium (eqn (1)). By rearranging the Nernst equation in terms of ammonia activity a_{NH_3} , a near-Nernstian slope of 59.3 mV per decade ($r^2 = 0.995$) was observed across the resulting $\log[\text{NH}_3]$ concentrations. This calibration captures the behavior of the sensor under typical aqueous environmental conditions, such as aquaculture or surface water monitoring, where NH_3 arises from NH_4^+ dissociation in buffered media.

To further verify the stability of the individual electrodes in the absence of an external reference electrode, open-circuit EMF drift experiments were conducted for both the NH_4^+ -ISE and H^+ -ISE in 50 mM Tris buffer for 4 hours. As shown in Fig. S1, the NH_4^+ -ISE (MWCNT-based) exhibited a drift of less than 1.3 mV h^{-1} , and the H^+ -ISE (PEDOT:PSS-based) showed a drift below 0.5 mV h^{-1} . Additionally, the reproducibility of slope and intercept values across three days is summarized in Table S1, confirming the stability and well-defined baseline potentials (E^0) of both electrodes. These results validate the application of the dual-ISE system without an external reference electrode.

Headspace calibration above NH_4Cl solution. To simulate environmental NH_3 volatilization (*e.g.*, from soil or wastewater), the sensor was placed in the headspace above closed containers containing 10^{-4} M NH_4Cl solutions. Upon equilibration, NH_3 partitions into the gas phase following Henry's Law:

$$P_{\text{NH}_3} = K_{\text{H}} \cdot a_{\text{NH}_3} \quad (6)$$

where K_{H} is the Henry's Law constant for NH_3 ($0.017 \text{ mol L}^{-1} \text{ atm}^{-1}$ at 25°C). The EMF signal in this configuration reflects the partial pressure of NH_3 gas above the aqueous phase and remains directly related to the dissolved ammonia activity. The response exhibited a well-defined Nernstian trend with a slope of 57.3 mV per decade ($r^2 = 0.997$) and a practical detection limit of $\sim 10^{-5}$ atm (corresponding to ~ 0.0069 ppm NH_3 in solution). This setup bridges the aqueous and gaseous environments and highlights the sensor's suitability for in-field deployment near open ammonia sources.

Dry gas calibration with NH_3/N_2 mixtures. In the third calibration mode, the sensor was placed in a sealed gas-tight chamber flushed with controlled mixtures of NH_3 and N_2 gases, simulating workplace or industrial air monitoring. Partial pressures of NH_3 were adjusted to 0.00001, 0.0001,

0.001, 0.01, and 0.1 atm, corresponding to 10, 100, 1000, 10 000, and 100 000 ppm (v/v), respectively. These values represent the volume fraction of ammonia in the gas phase and are aligned with occupational exposure standards.

Under these dry conditions, the EMF response remained rapid, stable, and highly linear with respect to $\log(P_{\text{NH}_3})$, exhibiting a slope of 60.9 mV per decade ($r^2 = 0.988$), consistent with ideal Nernstian behavior. Unlike conventional gas sensors that rely on slow permeation through membranes or internal buffers, this sensor responds instantly to changes in ammonia gas concentration due to the direct potentiometric measurement across the NH_4^+/H^+ pair. This makes it highly applicable for personal exposure monitoring, industrial leak detection, or confined space ammonia surveillance.

In comparison with commercial NH_3 gas sensor, Fig. 1 shows the response of a commercial NH_3 gas-sensing electrode under identical P_{NH_3} conditions. While the commercial sensor showed a reasonable response above 1000 ppm, its sensitivity diminished sharply below 100 ppm, and the slope was substantially near-Nernstian (< -58 mV per decade). These deviations arise due to limitations in gas permeation through the hydrophobic membrane and slower equilibration of the internal buffer system, consistent with earlier reports.^{38,39} In contrast, the dual-ISE setup enabled direct potentiometric sensing of NH_3 activity with no diffusion barrier, minimal hysteresis, and superior detection limits. The direct signal acquisition and absence of internal liquid junctions also contribu-

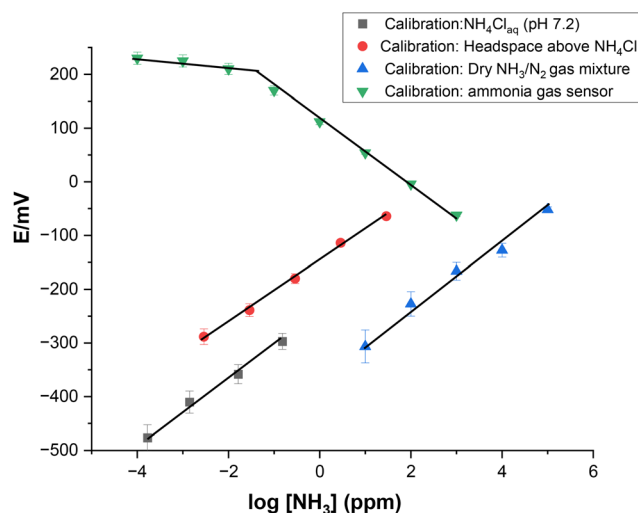


Fig. 1 Calibration curves of the all-solid-state NH_3 sensor under various experimental conditions. The sensor response (EMF, mV) is plotted against the logarithm of free ammonia concentration in ppm. Four calibration modes are presented: (■) aqueous NH_4Cl solutions at pH 7.2 (equilibrium-determined NH_3 activity), (●) headspace above 10^{-4} M NH_4Cl (NH_3 partitioned *via* Henry's law), (▲) dry NH_3/N_2 gas mixtures at controlled partial pressures, and (▼) a commercial ammonia gas sensor (Orion) used for comparison. Each configuration exhibits a linear Nernstian response across log-scale NH_3 concentrations, with slopes varying by detection mechanism and medium. The x-axis is plotted on a logarithmic scale to capture the broad dynamic range of ammonia concentrations across several orders of magnitude.

ted to improved mechanical stability and portability, desirable in field applications.^{40–42}

A comparative evaluation of the two solid-contact materials used in this study—PEDOT:PSS and MWCNTs—was conducted to assess their influence on sensor performance. As summarized in Table S2 (SI), both materials yielded near-Nernstian slopes and comparable detection limits. However, PEDOT:PSS-based electrodes exhibited faster response times ($t_{90\%} \approx 4$ s) and lower baseline drift (0.5 ± 0.1 mV h⁻¹) than their MWCNT counterparts ($t_{90\%} \approx 7$ s; drift = 1.3 ± 0.2 mV h⁻¹). These results support the use of PEDOT:PSS for applications requiring high signal stability, while MWCNTs offer competitive performance in scenarios prioritizing material flexibility or hydrophobicity.

Response dynamics and reversibility

As shown in Fig. 2, the proposed ion-selective NH₃ sensor exhibits a significantly faster response compared to the commercial ammonia gas probe. The solid-state NH₃ sensor stabilizes within 5 s ($t_{95\%}$) across a range of partial pressures ($P_{\text{NH}_3} = 0.0004$ – 0.0655 atm), while the commercial probe requires over 50–100 s for signal stabilization, particularly at low NH₃ levels. The delayed response in the commercial sensor is attributed to diffusion-limited transport of NH₃ gas through a hydrophobic membrane into an internal electrolyte containing pH indicators or buffers. This well-documented kinetic limitation results in signal lag and temporal averaging, reducing the utility of such sensors for dynamic or real-time applications.³⁸ At lower NH₃ concentrations, the slower diffusion rate and reduced partial pressure gradient across the membrane further exacerbate the delay, which also contributes to the near-

Nernstian behavior observed for the commercial probe in Fig. 1. In contrast, the all-solid-state NH₃ sensor avoids such membrane-based constraints by directly coupling an ammonium-selective electrode (NH₄⁺-ISE) with a pH-selective electrode (H⁺-ISE), thereby enabling potentiometric measurement of ammonia activity through the gas–liquid equilibrium $\text{NH}_4^+ \leftrightarrow \text{NH}_3 + \text{H}^+$. This dual-electrode configuration provides direct and rapid readout of NH₃ activity without the need for a diffusion or internal reference medium.

The sensor's dynamic reversibility was validated by exposing it to stepwise decreases in NH₃ partial pressure (Fig. 3). EMF stabilization occurred within 8–10 s even at low P_{NH_3} values (down to 0.0004 atm), with no significant hysteresis or baseline drift, confirming excellent reversibility and minimal memory effects. It is important to note that during these experiments, a gradual shift in the H⁺-ISE potential was observed, even under buffered conditions. This is not indicative of pH drift or sensor instability, but rather a thermodynamically expected consequence of the dynamic NH₄⁺/NH₃/H⁺ equilibrium. As NH₄⁺ dissociates to form NH₃ and H⁺, the proton activity at the membrane interface may transiently increase, leading to potential shifts. However, since our sensor measures the difference between the NH₄⁺ and H⁺ electrode potentials, this behavior is inherently accounted for in the EMF calculation. Therefore, the sensor output accurately reflects NH₃ activity, even under non-static proton conditions.

Collectively, these results establish the proposed dual-electrode ammonia sensor as a rapid, reversible, and thermo-

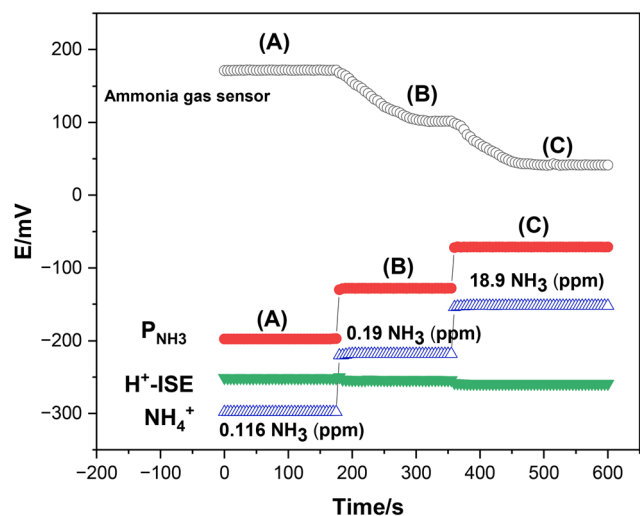


Fig. 2 Comparison of response time between the commercial NH₃ gas sensor, the NH₄⁺-selective electrode (NH₄⁺-ISE), and the H⁺-selective electrode (H⁺-ISE) coupled to the NH₃ sensing configuration in 0.1 M Tris–H₂SO₄ buffer at pH 7.2. The sensor systems were sequentially exposed to atmospheres equilibrated with increasing NH₃ partial pressures: (A) 0.0004 atm (0.116 ppm NH₃), (B) 0.0066 atm (1.91 ppm NH₃), and (C) 0.0655 atm (18.96 ppm NH₃).

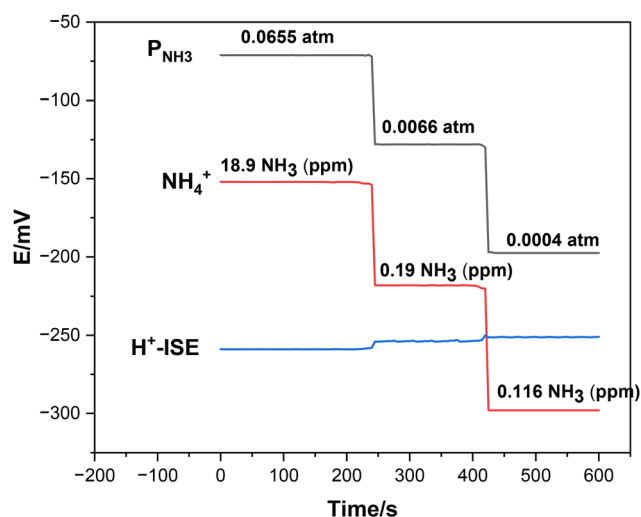


Fig. 3 Response time of the ion-selective NH₃ sensor to decreasing ammonia partial pressures (P_{NH_3}). The system was sequentially exposed to P_{NH_3} values of (A) 0.0655 atm, (B) 0.0066 atm, and (C) 0.0004 atm, corresponding to dissolved NH₃ concentrations of 18.9 ppm, 0.19 ppm, and 0.116 ppm, respectively. The pressure steps were applied in descending order to evaluate the dynamic behavior of the NH₄⁺-selective electrode (NH₄⁺-ISE, red), H⁺-selective electrode (H⁺-ISE, blue), and the commercial ammonia gas sensor (black) in 0.1 M Tris–H₂SO₄ buffer (pH 7.2). The observed drift in H⁺-ISE potential corresponds to expected proton release during NH₄⁺ dissociation and is compensated for in the final EMF calculation reflecting NH₃ activity.

dynamically well-defined platform for real-time NH_3 detection, significantly outperforming classical gas-sensing probes in response time, detection limit, and environmental adaptability.

Matrix effects and ionic strength stability

As shown in Fig. 4, when the sample solution was equilibrated with a fixed partial pressure of ammonia ($P_{\text{NH}_3} = 0.05 \text{ atm}$), the concentration of dissolved NH_3 in the system is governed by Henry's law and remains constant throughout the experiment. It should be noted that the sensor performance relies on the thermodynamic equilibrium of the $\text{NH}_4^+/\text{NH}_3/\text{H}^+$ system. Under real-world conditions involving rapid pH changes or ionic flux—such as those caused by mixing events or effluent discharges—temporary deviations from equilibrium may occur. These non-equilibrium effects can induce short-lived fluctuations in the EMF output. However, our experiments (e.g., Fig. 4) show that the dual-electrode system quickly re-equilibrates, typically within 30–60 seconds, depending on stirring and volume. As such, the sensor maintains accurate and stable NH_3 measurement shortly after disturbances, demonstrating robustness for environmental applications with dynamic conditions. This means that the NH_3 activity—and therefore the EMF response from the proposed NH_3 sensor—should remain unchanged during solution manipulations that do not affect the gas-phase equilibrium.

To assess the influence of ionic strength and matrix composition, the concentration of Na^+ was gradually increased

through stepwise additions of NaCl , covering the range from 10^{-5} to 1 M . Each addition altered the solution's ionic strength and alkalinity, which impacts the dissociation equilibrium of NH_4^+ and thereby modulates both pH and NH_4^+ activity. Consequently, the individual EMF readings of the H^+ -selective and NH_4^+ -selective electrodes shifted accordingly. The pH electrode responded with a systematic increase in potential, reflecting the alkalization of the solution due to the progressive shift of the $\text{NH}_4^+/\text{NH}_3$ equilibrium toward free NH_3 at higher pH. Similarly, the NH_4^+ electrode exhibited a potential decrease, consistent with a decrease in protonated species concentration. These changes confirm the dynamic re-equilibration of both species as governed by the ammonium ion equilibrium in eqn (1). However, and crucially, the calculated EMF difference, corresponding to P_{NH_3} , remained effectively constant following each equilibration step. This demonstrates that while pH and NH_4^+ activities shift with ionic strength and buffer composition, the NH_3 partial pressure—dictated by the controlled gas-phase environment—remains unchanged. The transient spikes observed in the P_{NH_3} trace after each NaCl addition are due to brief disturbances in the solution-phase equilibrium; these signals rapidly return to baseline once the system re-equilibrates with the gas phase, typically within 30–60 seconds depending on stirring efficiency and volume. This experiment illustrates the sensor's ability to monitor real-time re-equilibration kinetics of the $\text{NH}_3/\text{H}^+/\text{NH}_4^+$ system under gas-liquid equilibrium conditions. In contrast, the commercial NH_3 gas probe demonstrated minimal response to these rapid chemical shifts due to its long response time (>5 min). As such, it fails to capture fast transient dynamics and cannot resolve re-equilibration kinetics within the time-scale of environmental or laboratory perturbations. These results confirm the superior capability of the dual-ion-selective NH_3 sensor to provide stable, thermodynamically accurate P_{NH_3} readings even under fluctuating ionic strength conditions—critical for complex matrices such as seawater, wastewater, or biological fluids.

Selectivity behavior of the NH_3 sensor

The overall selectivity of the proposed ammonia sensor is determined primarily by the performance of the nonactin-based ammonium-selective membrane electrode, as the paired pH electrode is highly specific to hydrogen ions and exhibits negligible interference from other species. To rigorously evaluate the selectivity of the ammonium-selective membrane under conditions relevant to environmental and biological applications, a series of common cationic and anionic species were tested using the separate solution method at matched activity levels.⁴³ The EMF response of the NH_4^+ -selective electrode was recorded against a variety of potential interferents, including the monovalent and divalent cations Na^+ , K^+ , Mg^{2+} , and Ca^{2+} , and the anions Cl^- , NO_3^- , SCN^- , ClO_4^- , salicylate (Sal^-), carbonate (CO_3^{2-}), and hydrosulfide (HS^-). Among the tested cations, potassium (K^+) showed the closest behavior to NH_4^+ due to similar ionic radii and complexation behavior with nonactin; however, even in this case, the EMF response

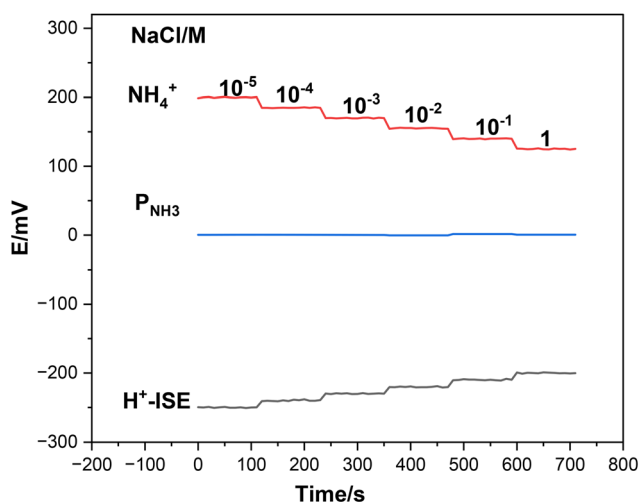


Fig. 4 Simultaneous monitoring of NH_4^+ , H^+ , and calculated P_{NH_3} in solution equilibrated with 0.05 atm NH_3 using a dual-ion-selective electrode configuration. Stepwise additions of NaCl were used to increase the Na^+ concentration from 10^{-5} M to 1 M , simulating matrix effects and ionic strength variation. The NH_4^+ -selective electrode (red trace) exhibited a gradual decrease in potential due to reduced protonated species activity under elevated ionic strength. The H^+ -selective electrode (black trace) showed an increasing EMF trend reflecting solution alkalization and the shift in $\text{NH}_4^+/\text{NH}_3$ equilibrium. In contrast, the calculated P_{NH_3} signal (blue trace) remained stable throughout, confirming the robustness of the dual-ISE NH_3 sensor under fluctuating ionic conditions.

Table 1 Potentiometric selectivity coefficients ($\log K_{i,j}^{\text{pot}}$) of the proposed NH_4^+ -selective electrode, determined using the Separate Solution Method (SSM) at matched activity levels

	Interfering ion, J										
$\log K_{i,j}^{\text{pot}}$	K^+	Na^+	Ca^{2+}	Mg^{2+}	Cl^-	NO_3^-	SCN^-	ClO_4^-	Sal^-	CO_3^{2-}	HS^-
	-1.1	-2.7	-4.2	-3.7	<-5.0	<-5.0	<-5.0	<-5.0	<-5.0	<-5.0	<-5.5

deviated significantly—by over three orders of magnitude—confirming that selectivity for NH_4^+ over K^+ remains acceptable for most natural water samples. Sodium (Na^+), magnesium (Mg^{2+}), and calcium (Ca^{2+}), which are present in relatively high concentrations in seawater ($\text{Na}^+ \approx 470$ mM, $\text{Mg}^{2+} \approx 50$ mM, $\text{Ca}^{2+} \approx 10$ mM), elicited negligible shifts in EMF across their activity ranges, confirming the high selectivity of the membrane toward ammonium over these background electrolytes. All selectivity coefficient values are presented in Table 1.

In addition to ionic interferents, we considered the potential influence of dissolved acidic gases, particularly CO_2 and H_2S , which may alter the proton activity and disrupt the $\text{NH}_4^+/\text{NH}_3$ equilibrium. While all experiments were conducted in buffered media (50 mM Tris, pH 7.2), literature reports suggest that exposure to ~ 0.05 atm CO_2 can induce a transient pH drop of ~ 0.2 units in similarly buffered solutions, leading to a reversible EMF shift of ~ 10 – 12 mV. For H_2S , the dominant aqueous species near neutral pH is HS^- , which contributes minimally to proton activity; this is consistent with the minimal EMF change observed for HS^- in our interference study (Table 1). These findings suggest that under typical environmental buffering, the dual-ISE system maintains reliable response. However, under unbuffered or highly variable gas exposure, transient shifts may occur and should be accounted for in practical deployments.

Regarding anions, although they are not expected to directly interfere with the cation-selective response of the membrane, their presence was tested to evaluate any indirect or membrane-interfacial effects. Chloride (Cl^-), nitrate (NO_3^-), thiocyanate (SCN^-), perchlorate (ClO_4^-), and salicylate showed no significant EMF change and thus no measurable interference. Carbonate (CO_3^{2-}), which may co-exist in alkaline samples or be introduced *via* dissolved CO_2 , also did not affect the membrane response. Of particular interest is the performance of the sensor in the presence of hydrogen sulfide, a compound frequently encountered in anaerobic environments such as sediments or stagnant waters. At neutral pH, hydrogen sulfide exists primarily as HS^- , which was found to be suppressed by over 3.5 orders of magnitude relative to NH_4^+ , confirming that the sensor maintains robust selectivity even in sulfide-rich matrices. This is especially relevant since traditional Severinghaus-type ammonia or CO_2 gas probes are known to suffer from H_2S interference due to the diffusion of neutral H_2S across gas-permeable membranes, leading to internal pH drift and erroneous readings. In summary, the data in Table 1 demonstrate that the nonactin-based ammonium-selective membrane exhibits excellent selectivity against both cationic and anionic interferents commonly present in natural waters,

wastewater, or biological fluids. This renders the dual-electrode NH_3 sensor highly suitable for direct deployment in unmodified complex matrices without the need for sample pre-treatment or separation steps.

pH effect and real-time ammonia monitoring

The NH_4^+ -selective electrode used in this sensor platform is inherently responsive to the activity of ammonium ions in the sample, while the associated pH electrode selectively measures hydrogen ion activity. During continuous and real-time monitoring experiments (*e.g.*, aquarium testing), both the individual electrode potentials ($E_{\text{NH}_4^+}$ and E_{H^+}) and their differential EMF were recorded. This dual readout strategy allowed us to identify the dominant species responsible for NH_3 fluctuations and to assess whether changes originated from pH shifts, ammonium concentration changes, or both. Since the calculated EMF is thermodynamically linked to NH_3 activity through the equilibrium relation in eqn (3), the system inherently accounts for simultaneous variation in NH_4^+ and H^+ , without requiring external reference electrodes or fixed pH conditions. Since the sensor EMF is based on the difference between the two electrodes ($\text{EMF} = E_{\text{NH}_4^+} - E_{\text{H}^+}$), the measured signal corresponds to the activity of dissolved NH_3 , which is related through the equilibrium shown in eqn (1). As the pH of the sample decreases below the pK_a of NH_4^+ (9.25), the equilibrium shifts toward NH_4^+ , and the proportion of free NH_3 diminishes exponentially. At sufficiently low pH (*e.g.*, below 6.0), this can lead to a diminished EMF response, and even potential interference from alkali or alkaline earth cations such as Na^+ and K^+ becomes more prominent due to reduced NH_3 signal. To assess this effect, the sample solution was equilibrated at a constant P_{NH_3} of 0.05 atm, and the pH was progressively lowered by HCl addition. The pH was adjusted using dropwise addition of HCl, and the values were monitored with a calibrated glass pH electrode. All measurements were carried out in the same Tris buffer solution to ensure that the observed EMF changes were exclusively due to pH variation and not buffer composition. As shown in Fig. 5, the ideal sensor response at fixed P_{NH_3} would remain constant across the pH range, indicated by the dashed line. However, the EMF decreased notably below pH 6 due to the reduction in free NH_3 concentration and the influence of matrix ions. These results define the lower operational pH limit of the sensor and suggest optimal performance in the pH range 6–9, where NH_3 activity is sufficiently high for robust detection.

To demonstrate the practical utility of the sensor, a fish-containing freshwater aquarium was used to monitor diurnal fluctuations in ammonia concentrations. Fish respiration,

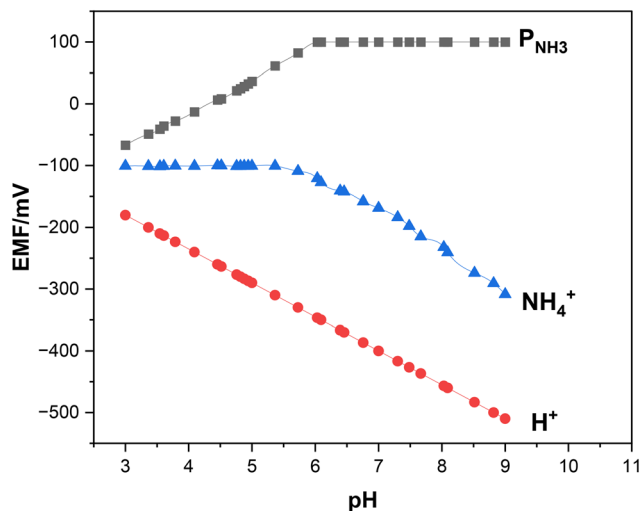


Fig. 5 Potentiometric response of the dual-electrode NH_3 sensor system as a function of pH at constant $P_{\text{NH}_3} = 0.05$ atm. The red circles represent the EMF of the H^+ -selective electrode (H^+ -ISE), the blue triangles represent the EMF of the NH_4^+ -selective electrode (NH_4^+ -ISE), which responds to changes in NH_4^+ activity as it equilibrates with NH_3 and H^+ , and the black squares represent the calculated EMF difference ($E_{\text{NH}_4^+} - E_{\text{H}^+}$), which reflects the activity of dissolved NH_3 .

waste excretion, and biological filtration induce dynamic pH and nitrogen cycling. The dual-electrode NH_3 sensor recorded dissolved ammonia levels continuously, and results were compared to a commercial Severinghaus-type probe under the same conditions. This setup mimics aquaculture or ornamental fish systems, where continuous NH_3 monitoring is essential for animal health and water quality management.

As shown in Fig. 6, the dual-electrode NH_3 sensor effectively recorded diurnal variations in ammonia concentration within a freshwater aquarium containing live fish. During the dark phase, increased CO_2 from fish respiration and reduced photosynthetic activity led to a drop in pH, shifting the $\text{NH}_4^+/\text{NH}_3$ equilibrium toward NH_4^+ and thereby elevating NH_3 activity. In contrast, during the light phase, aeration and biological filtration processes increased pH levels, promoting the conversion of NH_4^+ to NH_3 and resulting in a relative decrease in free ammonia activity. The ion-selective NH_3 sensor recorded NH_3 levels of $85.3 \pm 0.8 \mu\text{M}$ at the end of the dark phase and $58.2 \pm 0.7 \mu\text{M}$ at the end of the light phase. For comparison, the Severinghaus-type ammonia probe recorded $87.1 \pm 17.1 \mu\text{M}$ (night) and $60.8 \pm 2.0 \mu\text{mol L}^{-1}$ (day), with considerably higher signal variability and baseline drift, especially during nocturnal measurements.

These results highlight the sensor's ability to capture rapid fluctuations in ammonia levels with high temporal resolution and low drift, even in biologically active aquatic environments. The enhanced signal stability of the solid-state NH_3 sensor over the commercial gas-sensing probe is attributed to its membrane-free design and the absence of internal electrolyte solutions or diffusion-limited interfaces. The data confirm the sensor's practical suitability for continuous ammonia monitor-

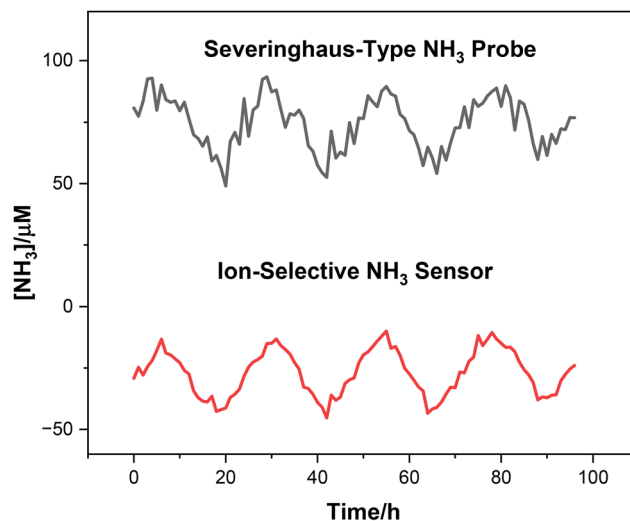


Fig. 6 Continuous monitoring of ammonia concentration in a fish-containing freshwater aquarium using a Severinghaus-type NH_3 probe (top trace, black) and an ion-selective NH_3 sensor (bottom trace, red) over a 96-hour period under light/dark cycling.

ing in aquaculture systems, fish tanks, and other dynamic aquatic settings where accurate and stable NH_3 detection is critical.

Conclusion

In conclusion, a potentiometric method based on the use of coupled ammonium- and hydrogen ion-selective electrodes was developed for the selective and reversible detection of dissolved ammonia (NH_3) in both aqueous solutions and equilibrated gas-phase environments. The sensor exhibited a near-Nernstian response with respect to NH_3 activity, with a detection limit sufficiently low to meet the requirements of most environmental, aquaculture, and clinical applications. The response time was significantly faster—by more than an order of magnitude—compared to conventional Severinghaus-type ammonia gas probes, enabling real-time monitoring of ammonia dynamics in complex systems. The dual-electrode configuration also provided a stable and matrix-independent response, allowing accurate NH_3 detection under varying ionic strengths and pH conditions without the need for gas-permeable membranes or internal filling solutions. Moreover, the individual signals from the NH_4^+ - and H^+ -selective electrodes may be used to extract additional information about ammonium concentration and pH, offering a multifunctional sensing platform. In such multi-analyte configurations, a reference electrode may be required to preserve potential stability across extended time periods or variable sample conditions. This sensor represents a robust and practical tool for on-site, continuous ammonia monitoring, with strong potential for deployment in aquatic systems, environmental assessments, and biological studies where fast and reliable ammonia quantification is essential. Potential pH perturbations caused

by exposure to acidic gases (*e.g.*, CO₂, H₂S) were evaluated and are expected to induce minor, reversible effects in buffered conditions; future work will consider housing or compensation strategies for use in more volatile environments. Furthermore, the independent monitoring of both NH₄⁺ and H⁺ potentials allow the system to operate effectively even under conditions where both pH and ammonium concentrations fluctuate simultaneously.

Author contributions

The listed authors contributed to this work as follows: conceptualization, A. H. K.; methodology, H. S. M. A. and A. H. K.; software, H. S. M. A.; validation, H. S. M. A. and A. H. K.; formal analysis, A. H. K.; investigation, H. S. M. A. and A. H. K.; resources, H. S. M. A.; data curation, H. S. M. A.; writing—original draft preparation, H. S. M. A. and A. H. K.; writing—review and editing, A. H. K.; visualization, H. S. M. A. and A. H. K.; supervision, A. H. K.; project administration, H. S. M. A. All authors have read and agreed to the published version of the manuscript.

Conflicts of interest

The authors declare that there are no competing financial or personal interests that could have appeared to influence the work reported in this manuscript.

Data availability

The data supporting the findings of this study are available from the corresponding author upon reasonable request.

Supplementary information is available. See DOI: <https://doi.org/10.1039/d5an00647c>.

Acknowledgements

The author H. S. M. Abd-Rabboh extends his appreciation to the University Higher Education Fund for funding this research work under the Research Support Program for Central labs at King Khalid University through project number CL/RP/9).

References

- 1 B. B. Jana, *Interact. Food, Agric. Environ. II*, 2010, 323.
- 2 X. Wang, A. P. Tsimpidi, Z. Luo, B. Steil, A. Pozzer, J. Lelieveld and V. A. Karydis, *EGU Sphere*, 2025, **2025**, 1–35.
- 3 X. Wang, J. Li, J. Chen, L. Cui, W. Li, X. Gao and Z. Liu, *Chemosphere*, 2020, **243**, 125328.
- 4 K. Lin, Y. Zhu, Y. Zhang and H. Lin, *Trends Environ. Anal. Chem.*, 2019, **24**, e00073.
- 5 L. O. Šraj, M. I. G. S. Almeida, S. E. Swearer, S. D. Kolev and I. D. McKelvie, *TrAC, Trends Anal. Chem.*, 2014, **59**, 83–92.
- 6 X. Guo, J. Chen, Y. Shen, H. Li and Y. Zhu, *TrAC, Trends Anal. Chem.*, 2024, **171**, 117519.
- 7 A. Biswas, B. Ghosh and R. S. Dey, *Langmuir*, 2023, **39**, 3810–3820.
- 8 K. Murugappan, J. Lee and D. S. Silvester, *Electrochem. commun.*, 2011, **13**, 1435–1438.
- 9 M. E. Lopez and G. A. Rechnitz, *Anal. Chem.*, 1982, **54**, 2085–2089.
- 10 L. Wang, Y. Cheng, S. Gopalan, F. Luo, K. Amreen, R. K. Singh, S. Goel, Z. Lin and R. Naidu, *ACS Sens.*, 2023, **8**, 1373–1390.
- 11 G. A. Crespo, *Electrochim. Acta*, 2017, **245**, 1023–1034.
- 12 L. Gao, Y. Tian, W. Gao and G. Xu, *Sensors*, 2024, **24**, 4289.
- 13 Y. Lyu, S. Gan, Y. Bao, L. Zhong, J. Xu, W. Wang, Z. Liu, Y. Ma, G. Yang and L. Niu, *Membranes*, 2020, **10**, 128.
- 14 M. Cuartero, N. Colozza, B. M. Fernández-Pérez and G. A. Crespo, *Analyst*, 2020, **145**, 3188–3210.
- 15 J. Schwarz, K. Trommer and M. Mertig, *Am. J. Anal. Chem.*, 2018, **9**, 591.
- 16 S. Krivačić, Ž. Boček, M. Zubak, V. Kojić and P. Kassal, *Talanta*, 2024, **279**, 126614.
- 17 A. H. Kamel and H. R. Galal, *Int. J. Electrochem. Sci.*, 2014, **9**, 4361–4373.
- 18 A. A. Aziz and A. H. Kamel, *Talanta*, 2010, **80**, 1356–1363.
- 19 S. S. M. Hassan, S. A. M. Marzouk, A. H. K. Mohamed and N. M. Badawy, *Electroanalysis*, 2004, **16**, 298–303.
- 20 F. T. C. Moreira, J. R. L. Guerreiro, V. L. Azevedo, A. H. Kamel and M. G. F. Sales, *Anal. Methods*, 2010, **2**, 2039–2045.
- 21 S. S. M. Hassan, A. H. Kamel and M. A. Fathy, *Anal. Chim. Acta*, 2022, **1227**, 340239.
- 22 A. H. Kamel, N. H. Ashmawy, T. A. Youssef, M. Elnakib, H. Abd El-Naby and H. S. M. Abd-Rabboh, *Electroanalysis*, 2023, **35**, e202200436.
- 23 H. S. M. Abd-Rabboh, A. El-Galil, E. Amr, E. A. Elsayed, A. Y. A. Sayed and A. H. Kamel, *RSC Adv.*, 2021, **11**, 12227–12234.
- 24 Y. Shao, Y. Ying and J. Ping, *Chem. Soc. Rev.*, 2020, **49**, 4405–4465.
- 25 P. Wang, H. Liu, S. Zhou, L. Chen, S. Yu and J. Wei, *Molecules*, 2023, **28**, 5503.
- 26 M. A. Fathy and P. Bühlmann, *Biosensors*, 2025, **15**, 51.
- 27 J. Hu, A. Stein and P. Bühlmann, *TrAC, Trends Anal. Chem.*, 2016, **76**, 102–114.
- 28 J. A. Galvão, A. Matthiensen, M. Oetterer, Y. Moliner-Martínez, R. A. Gonzalez-Fuenzalida, M. Muñoz-Ortuño, R. Herráez-Hernández, J. Verdú-Andrés, C. Molins-Legua and P. C. Falcó, *Handb. water Anal.*, 2013, **5**, 249.
- 29 Y. Wen, Y. Mao, Z. Kang and Q. Luo, *Measurement*, 2019, **137**, 98.
- 30 M. T. Ghoneim, A. Nguyen, N. Dereje, J. Huang, G. C. Moore, P. J. Murzynowski and C. Dagdeviren, *Chem. Rev.*, 2019, **119**, 5248–5297.
- 31 T. Li, *Field-based Sensing Techniques for Real-time Monitoring Wastewater Quality and Free Ammonia*, 2016, <https://research->

- repository.griffith.edu.au/server/api/core/bitstreams/e90cd600-1e47-5dfc-ad05-a48d665ab90e/content.
- 32 K. Gruiz, É. Fenyvesi, M. Molnár, V. Feigl, E. Vaszita and M. Tolner, in *Engineering Tools for Environmental Risk Management*, CRC Press, 2017, pp. 245–342.
 - 33 Á. Molinero-Fernandez, Q. Wang, X. Xuan, Å. Konradsson-Geuken, G. A. Crespo and M. Cuartero, *ACS Sens.*, 2024, **9**, 361–370.
 - 34 H. S. Hisham and A. H. Kamel, *Anal. Sci.*, 2020, **36**, 1359–1364.
 - 35 M. M. El-Beshlawy, F. M. Abdel-Haleem, A. H. Kamel and A. Barhoum, *Chemosensors*, 2022, **11**, 3.
 - 36 A. G. Eldin, A. E.-G. E. Amr, A. H. Kamel and S. S. M. Hassan, *Molecules*, 2019, **24**, 1392.
 - 37 A. H. Kamel, S. Ezzat, M. A. Ahmed, A. E.-G. E. Amr, A. A. Almehizia and M. A. Al-Omar, *Biomolecules*, 2020, **10**, 251.
 - 38 J. W. Severinghaus and A. F. Bradley, *J. Appl. Physiol.*, 1958, **13**, 515–520.
 - 39 K. Y. Chumbimuni-Torres, E. Bakker and J. Wang, *Electrochem. commun.*, 2009, **11**, 1964–1967.
 - 40 Y. Liu, H. Zhu, L. Xing, Q. Bu, D. Ren and B. Sun, *Nanoscale*, 2023, **15**, 6025–6051.
 - 41 W. Gao, X. Xie and E. Bakker, *ACS Sens.*, 2020, **5**, 313–318.
 - 42 R. Athavale, I. Kokorite, C. Dinkel, E. Bakker, B. Wehrli, G. A. Crespo and A. Brand, *Anal. Chem.*, 2015, **87**, 11990–11997.
 - 43 E. Bakker, *J. Electrochem. Soc.*, 1996, **143**, L83–L85.